Front. Optoelectron. 2018, 11(4): 367–374
https://doi.org/10.1007/s12200-018-0835-8

RESEARCH ARTICLE

$BiOI/WO_3$ photoanode with enhanced photoelectrochemical water splitting activity

Weina SHI[1,2], Xiaowei LV[1], Yan SHEN (✉)[1]

1 Wuhan National Laboratory for Optoelectronics, Huazhong University of Science and Technology, Wuhan 430074, China
2 College of Chemistry and Chemical Engineering, Xinxiang University, Xinxiang 453003, China

Abstract This work reports on a novel $BiOI/WO_3$ composite photoanode, which was fabricated by depositing BiOI onto a WO_3 nanoflake electrode through a electrodeposition method. The photoelectrochemical (PEC) activity of the $BiOI/WO_3$ electrode for water splitting under visible-light irradiation was evaluated. The results show that the $BiOI/WO_3$ photoanode achieved a photocurrent density of 1.21 $mA \cdot cm^{-2}$ at 1.23 V vs. reversible hydrogen electrode (RHE), which was higher than that of the bare WO_3 nanoflake electrode (0.67 $mA \cdot cm^{-2}$). The enhanced PEC acticity of $BiOI/WO_3$ for water splitting can be attributed to the expansion of light absorption range as well as the facilitated separation of photo-generated carriers.

Keywords photoelectrochemistry, WO_3, BiOI, water splitting

1 Introduction

Photoelectrodes of semiconductor oxides have been widely investigated for photoelectrochemical (PEC) water splitting for hydrogen production [1–7]. Recently, great attentions have been attracted for the n-type WO_3 photoanode, which has favorable valence band edge (3.0 eV versus normal hydrogen electrode), moderate hole diffusion length (~150 nm) and high electron mobility (~12 $cm^2 \cdot V^{-1} \cdot s^{-1}$) [8]. However, its PEC property is always limited by the relatively narrow absorption band (E_g = 2.5 – 2.8 eV), rapid recombination of photo-generated electron-hole pairs and tardy kinetics of holes [9]. WO_3 photoanode is not suitable for efficient PEC water oxidation unless credible methods can be developed to improve its visible light absorption capacity and promote the separation of photo-generated electron-hole pairs [10].

Various strategies have been employed to solve the above mentioned problems, including doping [11], nanostructure engineering, combination of semiconductors with small band gaps and so on [12–14]. For the nanostructured electrodes such as one dimensional nanorods, nanotubes and two dimensional nanoflakes, direct electrical pathways could be obtained for the photo-generated charges, and the diffusion lengths of the minority carriers could also be reduced, which lead to superior charge separation and transportation and thus excellent PEC properties [15]. For example, Amano et al. reported a 3.6 μm-thick WO_3 film consisting of perpendicularly oriented crystalline flakes fabricated with hydrothermal method, which exhibited a much larger photocurrent density of ~ 2 $mA \cdot cm^{-2}$ than the nanocrysalline WO_3 thin film at 1.2 V vs. Ag/AgCl electrode in 0.1 $mol \cdot L^{-1}$ Na_2SO_4 electrolyte [16]. Although the construction of nanostructured electrodes could enhance the separation of photogenerated carriers, the light absorption range of bare WO_3 was limited due to its inherent nature. The design of semiconductor composite was the most widely approach to develop photoelectrocatalytic materials in the past few decades. Among the numerous semiconductor composites, the p-n heterostructured systems with a staggered (Type II) band alignment have drawn much attention due to their enhanced efficient charge separation. In the composite system, materials with small band gaps could be used to broaden its light absorption range [10,17]. BiOX (X = Cl, Br, I) is a promising candidate semiconductor, due to the strong internal electric fields from a layered structure with $[Bi_2O_2]$ slabs interleaved with double halogen atom slabs along the [0 0 1] direction, leading to increase effective separation of the electron-hole pairs [18]. Among the BiOX semiconductors, BiOI has the smallest band-gap (1.8 eV) which could be motivated under most of the visible light range,

Received May 17, 2018; accepted June 20, 2018

E-mail: ciac_sheny@mail.hust.edu.cn

Special Issue—Energy Optoelectronics

with a BiOI modification can effectively enhance the PEC properties of the semiconductor photoelectrodes, such as BiOI/ZnO [19], BiOI/TiO_2 [20], BiOI/$BiVO_4$ [21]. However, there are few works focusing on the preparation and property of BiOI/WO_3 electrode for PEC water splitting.

In our work, we fabricated WO_3 nanoflakes by a seed-mediated hydrothermal method, which were uniformly distributed on the F doped SnO_2 substrate. Subsequently, BiOI were deposited through an electrodeposition method, and crossed network structure for the BiOI/WO_3 electrode was thus obtained. The as-prepared BiOI/WO_3 nanocomposite electrode exhibited a significantly improved photocurrent density in Na_2SO_4 solution under AM 1.5G illumination. The enhanced activity was mainly ascribed to the decoration of BiOI, which expanded light absorption range and facilitated separation of photo-generated carriers for the BiOI/WO_3 electrode.

2 Experimental section

2.1 Preparation of WO_3 photoanode

The WO_3 nanoflake photoanode was synthesized by hydrothermal reaction with seed-mediating according to our previously reported process [22]. The seed layer was deposited onto F doped SnO_2 (FTO) substrate by spin coating followed by annealing. The H_2WO_4 solution for the spin-coating process was prepared by dissolving H_2WO_4 (2.5 g) and poly(vinyl alcohol) (1 g) into of H_2O_2 (30 wt. %, 34 mL). Another H_2WO_4 solution was prepared by adding H_2WO_4 (2.5 g) and H_2O_2 (30 wt. %, 34 mL) into deionized water (50 mL), which was heated at 95°C to form a clear solution and then diluted to a concentration of 0.05 mol·L^{-1} for the solvothermal process. The WO_3 nanoflake film was grown by adding urea (0.02 g), oxalic acid (0.02 g), HCl (6 mol·L^{-1}, 0.5 mL) and H_2WO_4 solution (0.05 mol·L^{-1}, 3 mL) into acetonitrile (12.5 mL). The mixture was then transferred into a Teflonlined autoclave containing the seeded FTO substrate and then maintained at 180°C for 2 h. The resulting substrate after solvothermal process was washed with deionized water and dried with nitrogen flow, and then annealing at 500°C for 2 h in air to obtain the WO_3 photoanode.

2.2 Preparation of BiOI/WO_3 photoanode

The BiOI/WO3 photoanode was synthesized by an electrodeposition method [23]. In a typical process, a solution containing $Bi(NO_3)_3 \cdot 5H_2O$ (0.04 mol·L^{-1}) and KI (0.4 mol·L^{-1}) was adjusted to pH 1.7 by adding HNO_3, and then 20 mL of absolute ethanol containing p-benzoquinone (0.23 mol·L^{-1}) was added into the above solution with vigorously stirring for a few minutes at room temperature. The WO_3 electrode, Ag/AgCl electrode and Pt wire were served as the working electrode, reference electrode and counter electrode, respectively. Then BiOI was electrodeposited at −0.1 V vs. Ag/AgCl for different deposition times (5 − 25 s). The optimal deposition time was 15 s, and the corresponding photocurrent density was 1.21 mA·cm^{-2} at 1.23 V vs. reversible hydrogen electrode (RHE).

2.3 Sample characterization

X-ray diffraction (XRD) patterns of the electrodes were collected on an X-ray diffractometer (X' Pert PRO, PANalytical B.V.) using Cu Kα source radiation (1.540598 Å). Scanning electron microscopy (SEM, Nova NanoSEM 450, FEI) was used to investigate the surface morphologies of the samples. X-Ray photoelectron spectroscopy (XPS, AXIS-ULTRA DLD-600W, Shimdzu) was obtained to investigate chemical states of the samples. Raman spectra were recorded on a Raman spectrometer (LabRAM HR800) using a 532 nm laser as excitation source. UV-visible absorption spectra were obtained using a spectrophotometer (UV-3600, Shimdzu).

2.4 Photoelectrochemical measurements

PEC properties were investigated in a standard three-electrode configuration using CHI 630D electrochemical workstation (Chenhua, Shanghai, China). The as-synthesized samples acted as the working electrode, Ag/AgCl electrode and Pt wire as the reference electrode and counter electrode, respectively. 0.5 mol·L^{-1} of Na_2SO_4 solution was used as the electrolyte. All potentials were converted to RHE according to the Nernst equation: $E_{RHE} = E_{Ag/AgCl} + E^{\Theta}Ag/AgCl + (0.059 \times pH)$, where $E^{\Theta}Ag/AgCl$ is 0.197 V at 25°C. A gas chromatography ((Trustworthy Instrument, GC-2020N, China) with argon as a carrier gas was used for the analysis of the evolved gas. Electrochemical impedance spectroscopy (EIS) measurement was performed using an electrochemical impedance analyzer (CHI-920C) over a frequency range between 100 kHz and 0.1 Hz with an AC voltage magnitude of 5 mV amplitude at a bias potential of 1.23 V (vs. RHE).

3 Results and discussion

XRD measurements were carried out to determine the crystal phase of the samples. Figure 1(a) shows the XRD patterns of the WO_3, BiOI and BiOI/WO_3 electrodes. After subtracting the diffraction peaks of FTO substrate, all other peaks in the XRD pattern of BiOI/WO_3 electrode can be indexed into tetragonal BiOI (JCPDS No. 00-010-0445) and monoclinic WO_3 (JCPDS No. 00-043-1035) [24,25]. The Raman spectra of BiOI, WO_3 and BiOI/WO_3 were presented in Fig. 1(b). The strong peaks at 85 and 147 cm^{-1} are assigned to Bi-I vibration of BiOI [21]. The peaks at

715 and 806 cm^{-1} are ascribed to W-O bending (δ) and W-O stretching (ν) modes respectively. The peaks at 272 and 326 cm^{-1} correspond to the bending δ (O-W-O) vibrations, and the peak at 135 cm^{-1} are assigned to the lattice vibrations of WO_3 [26].

The SEM images of WO_3 and BiOI/WO_3 electrodes were depicted in Fig. 2. Figure 2(a) suggests that the pristine WO_3 sample displays uniform and vertically aligned nanoflakes. The SEM images in Fig. 2(b) clearly revealed the successful deposition of BiOI sheets, which attached onto the surfaces of WO_3 nanoflakes and formed crossed networks. The coating of BiOI caused an obvious color change from pale yellow to orange (digital photographs shown in the inset of Fig. 2), identifying the formation of BiOI/WO_3 composite electrode.

The chemical states of the samples are investigated by XPS. Figure 3 shows the high-resolution XPS spectra of BiOI/WO_3 electrode. As shown in Fig. 3(a), the two peaks with binding energy of 38.0 and 35.9 eV correspond well with the characteristic W $4f_{5/2}$ and W $4f_{7/2}$ of W^{6+} in WO_3, respectively [27]. Two strong peaks located at 164.4 and 159.0 eV in Fig. 3(b) are attributed to Bi $4f_{5/2}$ and Bi $4f_{7/2}$ of Bi^{3+} in BiOI, which are in agreement with the reported values [19]. The peaks centered at 630.4 and 618.9 eV in Fig. 3(c) are assigned to I $3d_{3/2}$ and I $3d_{5/2}$, respectively [18]. The O 1s spectrum in Fig. 3(d) could be deconvoluted into three peaks, which are related to Bi-O bonds (530.4 eV) of BiOI, W-O bonds (530.9 eV) of WO_3 and O-H bonds (531.9 eV) of the surface-adsorbed water, respectively [28–30].

Figure 4(a) shows the UV-visible absorption spectra of the WO_3, BiOI and BiOI/WO_3 electrodes. Bare WO_3 nanoflakes exhibit intrinsic absorption in the wavelength of 300 – 450 nm. While, a rather broad absorption range of 300 – 630 nm was observed for the BiOI/WO_3 composite, which was due to the good visible light response of BiOI. Furthermore, the indirect bandgaps of BiOI and WO_3 were determined by plotting the square root of the absorption

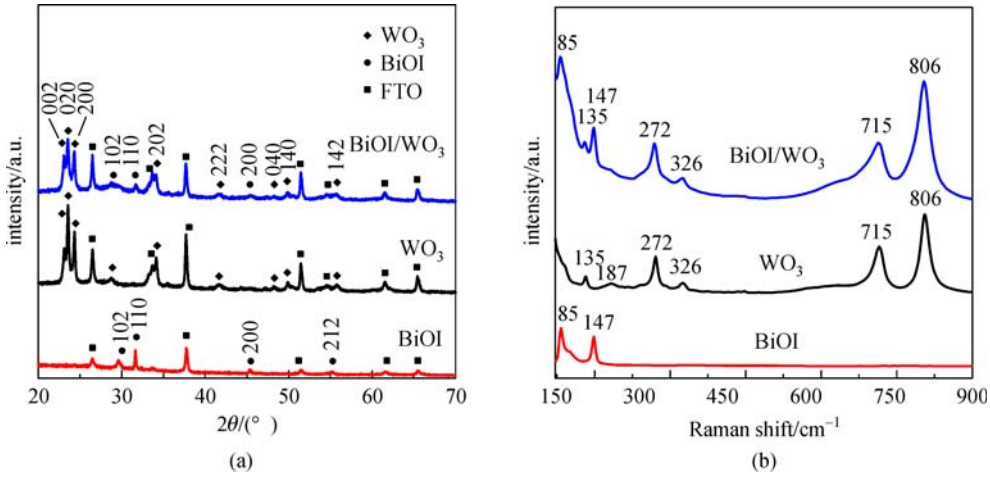

Fig. 1 (a) XRD patterns of BiOI, WO_3 and BiOI/WO_3; (b) Raman spectra of BiOI, WO_3 and BiOI/WO_3

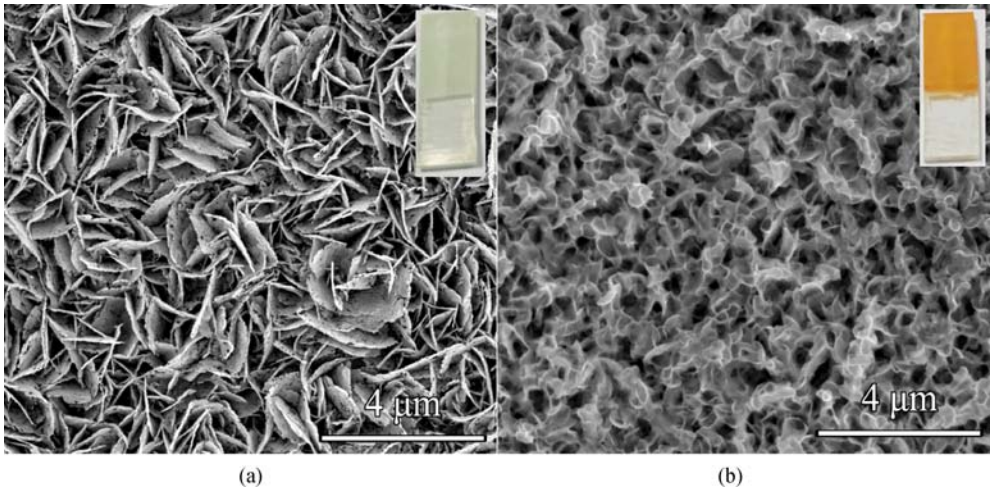

Fig. 2 SEM images of WO_3 (a) and BiOI/WO_3 (b) electrodes and their digital photographs (inset)

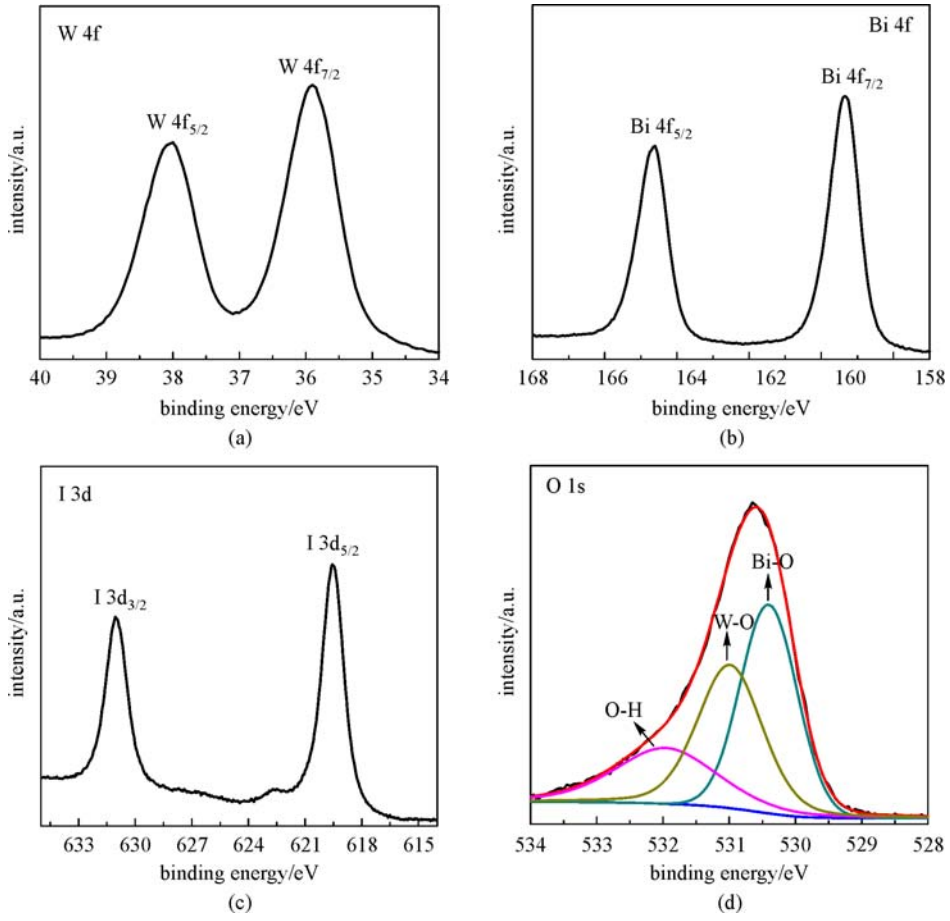

Fig. 3 High-resolution XPS spectra of the BiOI/WO_3 electrode: (a) W 4f, (b) Bi 4f, (c) I 3d and (d) O 1s

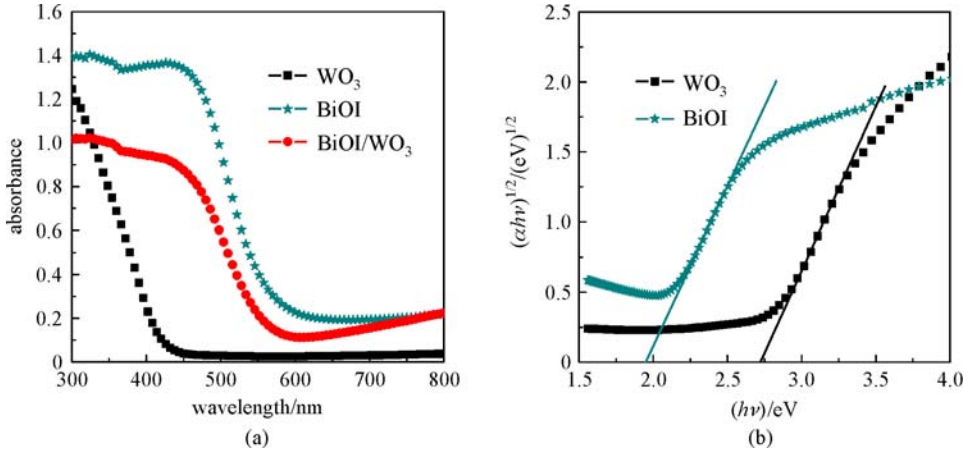

Fig. 4 (a) UV-visible absorption spectra of BiOI, WO_3 and BiOI/WO_3 electrodes; (b) Tauc plots converted from the UV-visible absorption spectra for BiOI and WO_3

energies against the photon energies. By extrapolating the linear portions to zero (Fig. 4(b)), the band gaps were estimated to be 1.95 and 2.72 eV for BiOI and WO_3, respectively, which are consistent with previous reports [31].

Linear sweep voltammogram (LSV) measurements were conducted in 0.5 mol·L^{-1} Na_2SO_4 electrolyte to evaluate the PEC response of the samples. As shown in Fig. 5(a), both of the samples show negligible dark current densities. Upon illumination, the BiOI/WO_3 composite electrode

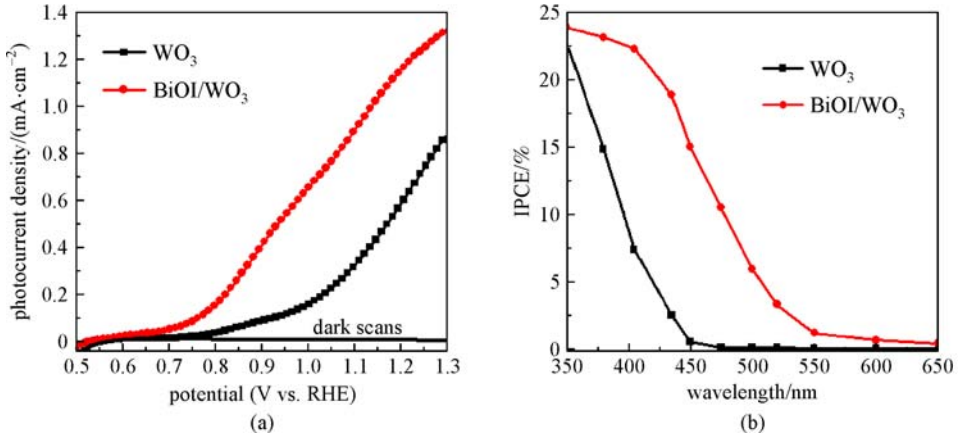

Fig. 5 (a) LSV scans of the WO_3 and BiOI/WO_3 electrodes in 0.5 mol·L^{-1} Na_2SO_4 electrolyte; (b) IPCE plots of the WO_3 and BiOI/WO_3 electrodes at 1.23 V vs. RHE in 0.5 mol·L^{-1} Na_2SO_4 electrolyte

achieved a photocurrent density of 1.21 mA·cm^{-2} at 1.23 V vs. RHE, which was 1.81 times as high as that of the pristine WO_3 nanoflakes (0.67 mA·cm^{-2}). Figure 5(b) depicted the incident photon to current conversion efficiency (IPCE) spectra of the pristine WO_3 and as-prepared BiOI/WO_3 electrodes at 1.23 V vs. RHE. As can be seen, the WO_3 electrode exhibited significant photocurrent response in the wavelength range of 350 – 450 nm, which was due to its intrinsic absorption. An obvious red-shift up to approximately 600 nm of the IPCE spectrum was observed for the BiOI/WO_3 composite electrode, indicating the visible-light response of BiOI. Furthermore, the IPCE values for the BiOI/WO_3 composite electrode were higher than those of bare WO_3. In particular, the IPCE values at 405 nm for the WO_3 and BiOI/WO_3 electrodes reached 7.3% and 22.2%, respectively. These results indicated that the modification of BiOI improved the PEC activity of WO_3.

Figure 6(a) shows the photocurrent densities of the obtained electrodes measured at 1.23 V vs. RHE in 0.5 mol·L^{-1} Na_2SO_4 electrolyte. The photocurrent of the bare WO_3 electrode attenuated quickly at the initial time, and lost 53% of the pristine value within 2000 s. However, the BiOI/WO_3 electrode exhibited a smaller attenuation of 28% as compared with that of the bare WO_3. Furthermore, the gaseous products of the WO_3 and BiOI/WO_3 electrodes were measured as a function of time at 1.23 V vs. RHE in 0.5 mol·L^{-1} Na_2SO_4 electrolyte. As can be seen in Fig. 6 (b), the amounts of H_2 and O_2 were close to the theoretical amounts determined by integrating the measured photocurrent over time. What's more, the proportion of evolved H_2 and O_2 was 2:1, indicating that the observed photocurrent is real water splitting photocurrent, rather than due to photodegradation.

Electrochemical impedance spectroscopy (EIS) measurements were implemented to study the interface charge transport properties of the electrodes. The charge-transfer resistance at the electrode-electrolyte interface can be

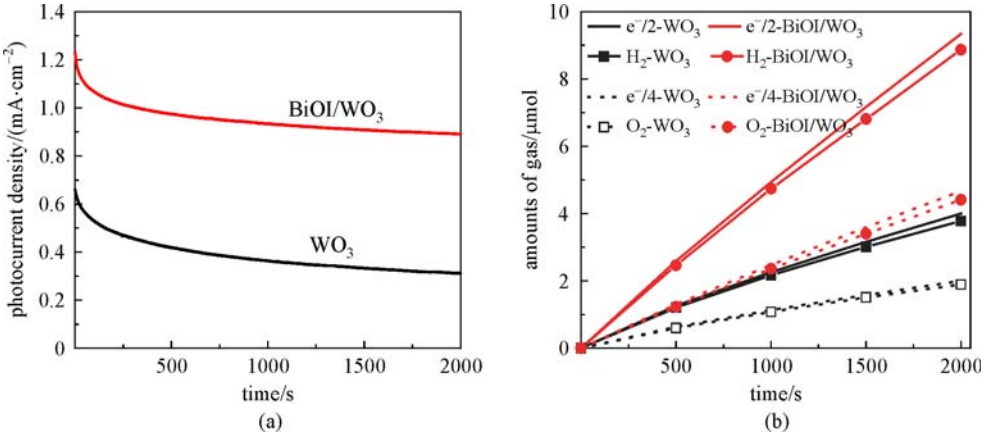

Fig. 6 Photocurrent density-time curves (a) and amounts of the theoretical and actual evolved gas (b) for the WO_3 and BiOI/WO_3 electrodes in 0.5 mol·L^{-1} Na_2SO_4 electrolyte

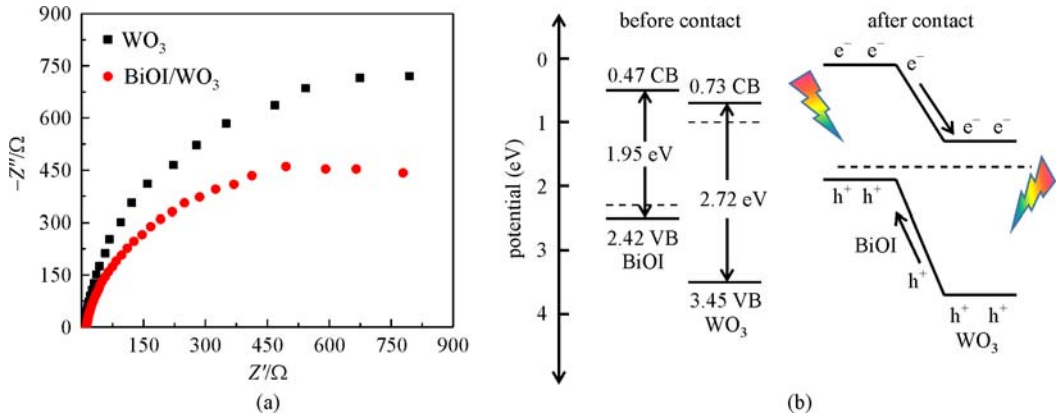

Fig. 7 (a) EIS Nyquist plots of WO_3 and BiOI/WO_3 electrodes measured at an applied bias of 1.23 V vs. RHE under AM 1.5G illumination; (b) schematic diagrams of the band energy of BiOI and WO_3 before and after contact

reflected from the semicircle in the Nyquist plots [32]. As shown in Fig. 7(a), the BiOI/WO_3 electrode exhibited a smaller semicircle as compared with that of WO_3, and it indicated that the introduction of BiOI led to an efficient separation of the electron-hole pairs for the composite electrode, in accordance with its improved PEC activity. Furthermore, the band energies of BiOI and WO_3 were also investigated. The conduction band (CB) and valence band (VB) edge at the point of zero charge for a semiconductor can be determined from the empirical equation [21]:

$$E_{VB} = X - E_e + 0.5E_g,$$

$$E_{CB} = E_{VB} - E_g,$$

where E_{VB} is the valence band edge potential, and E_e is the energy of free electrons on the hydrogen scale (~4.5 eV). X and E_g are the electronegativity and band-gap energy of the semiconductor, respectively. The X values of BiOI and WO_3 are 5.94 and 6.59 eV. As shown in Fig. 7(b), pristine BiOI and WO_3 owned their respective band energies before contact, which were obtained from the above UV-visible absorption spectra. When these two semiconductors are in contact, the photo-generated electrons and holes will be generated both in BiOI and WO_3 as the solar light illuminate on the BiOI/WO_3. The holes in WO_3 diffuse to BiOI, and caused efficient separation for the photo-generated electrons and holes. The recombination process is thus remarkably suppressed, leading to improved PEC water splitting activity.

4 Conclusion

In summary, we have successfully fabricated a WO_3 nanoflake electrode by a seed-mediated solvothermal method, followed by loading with BiOI through electro-depositing. The novel BiOI/WO_3 nanocomposite electrode achieved an enhanced PEC activity for water splitting, which may be attributed to the expansion of light absorption range as well as the facilitated separation of photo-generated carriers. These findings prove that the BiOI/WO_3 photoanode is a promising candidate for PEC water oxidation.

Acknowledgements This work was financially supported by the National Natural Science Foundation of China (NSFC) Major International (Regional) Joint Research Project NSFC-SNSF (Grant No. 51661135023), NSFC (Grant No. 21673091), the National Basic Research Program (973 Program) of China (No. 2014CB643506), the Fundamental Research Funds for the Central Universities (HUST: 2016YXMS031), the Director Fund of the WNLO, the Open Funds of the State Key Laboratory of Electroanalytical Chemistry (No. SKLEAC201607), Key Scientific and Technological Project of Henan Province (No. 182102311084). The authors thank the Analytical and Testing Center of HUST and the Center for Nanoscale Characterization & Devices (CNCD), WNLO-HUST for the measurements.

References

1. Kim H, Monllor-Satoca D, Kim W, Choi W. N-doped TiO_2 nanotubes coated with a thin TaO_xN_y layer for photoelectrochemical water splitting: dual bulk and surface modification of photoanodes. Energy & Environmental Science, 2015, 8(1): 247–257
2. Fan X, Wang T, Gao B, Gong H, Xue H, Guo H, Song L, Xia W, Huang X, He J. Preparation of the TiO_2/graphic carbon nitride core-shell array as photoanode for efficient photoelectrochemical water splitting. Langmuir, 2016, 32(50): 13322–13332
3. Ding D, Dong B, Liang J, Zhou H, Pang Y, Ding S. Solvothermal-etching process induced Ti-doped Fe_2O_3 thin film with low turn-on voltage for water splitting. ACS Applied Materials & Interfaces, 2016, 8(37): 24573–24578
4. Feng X, Chen Y, Qin Z, Wang M, Guo L. Facile fabrication of sandwich structured WO_3 nanoplate arrays for efficient photoelectrochemical water splitting. ACS Applied Materials & Interfaces, 2016, 8(28): 18089–18096

5. Yan L, Zhao W, Liu Z. 1D ZnO/$BiVO_4$ heterojunction photoanodes for efficient photoelectrochemical water splitting. Dalton Transactions (Cambridge, England), 2016, 45(28): 11346–11352
6. Fan X, Wang T, Guo Y, Gong H, Xue H, Guo H, Gao B, He J. Synthesis of ordered mesoporous TiO_2-Carbon-CNTs nanocomposite and its efficient photoelectrocatalytic methanol oxidation performance. Microporous and Mesoporous Materials, 2017, 240: 1–8
7. Xue H, Wang T, Gong H, Guo H, Fan X, Gao B, Feng Y, Meng X, Huang X, He J. Constructing ordered three-dimensional channels of TiO_2 for enhanced visible-light photo-catalytic performance of CO_2 conversion induced by Au nanoparticles. Chemistry, an Asian Journal, 2018, 13(5): 577–583
8. Berak J M, Sienko M J. Effect of oxygen-deficiency on electrical transport properties of tungsten trioxide crystals. Journal of Solid State Chemistry, 1970, 2(1): 109–133
9. Mi Q, Zhanaidarova A, Brunschwig B S, Gray H B, Lewis N S. A quantitative assessment of the competition between water and anion oxidation at WO_3 photoanodes in acidic aqueous electrolytes. Energy & Environmental Science, 2012, 5(2): 5694–5700
10. Li Y, Zhang L, LiuR, Cao Z, Sun X, Liu X, Luo J. WO_3@α-Fe_2O_3 heterojunction arrays with improved photoelectrochemical behavior for neutral pH water splitting. ChemCatChem, 2016, 8(17): 2765–2770
11. Zhang T, Zhu Z, Chen H, Bai Y, Xiao S, Zheng X, Xue Q, Yang S. Iron-doping-enhanced photoelectrochemical water splitting performance of nanostructured WO_3: a combined experimental and theoretical study. Nanoscale, 2015, 7(7): 2933–2940
12. Su J, Guo L, Bao N, Grimes C A. Nanostructured $WO_3/BiVO_4$ heterojunction films for efficient photoelectrochemical water splitting. Nano Letters, 2011, 11(5): 1928–1933
13. Boudoire F, Toth R, Heier J, Braun A, Constable E C. Photonic light trapping in self-organized all-oxide microspheroids impacts photoelectrochemical water splitting. Energy & Environmental Science, 2014, 7(8): 2680–2688
14. Solarska R, Królikowska A, Augustyński J. Silver nanoparticle induced photocurrent enhancement at WO_3 photoanodes. Angewandte Chemie International Edition, 2010, 49(43): 7980–7983
15. Su J, Feng X, Sloppy J D, Guo L, Grimes C A. Vertically aligned WO_3 nanowire arrays grown directly on transparent conducting oxide coated glass: synthesis and photoelectrochemical properties. Nano Letters, 2011, 11(1): 203–208
16. Amano F, Li D, Ohtani B. Fabrication and photoelectrochemical property of tungsten(vi) oxide films with a flake-wall structure. Chemical Communications (Cambridge, England), 2010, 46(16): 2769–2771
17. Mali M G, Yoon H, Kim M, Swihart M T, Al-Deyab S S, Yoon S S. Electrosprayed heterojunction $WO_3/BiVO_4$ films with nanotextured pillar structure for enhanced photoelectrochemical water splitting. Applied Physics Letters, 2015, 106(15): 151603
18. Ye L, Liu X, Zhao Q, Xie H, Zan L. Dramatic visible light photocatalytic activity of MnO_x–BiOI heterogeneous photocatalysts and the selectivity of the cocatalyst. Journal of Materials Chemistry A, Materials for Energy and Sustainability, 2013, 1(31): 8978–8983
19. Kuang P Y, Ran J R, Liu Z Q, Wang H J, Li N, Su Y Z, Jin Y G, Qiao S Z. Enhanced photoelectrocatalytic activity of BiOI nanoplate-zinc oxide nanorod p-n heterojunction. Chemistry (Weinheim an der Bergstrasse, Germany), 2015, 21(43): 15360–15368
20. Park H, Bak A, Ahn Y Y, Choi J, Hoffmannn M R. Photoelectrochemical performance of multi-layered BiO_x-TiO_2/Ti electrodes for degradation of phenol and production of molecular hydrogen in water. Journal of Hazardous Materials, 2012, 211–212: 47–54
21. Ye K H, Chai Z, Gu J, Yu X, Zhao C, Zhang Y, Mai W. BiOI–$BiVO_4$ photoanodes with significantly improved solar water splitting capability: p–n junction to expand solar adsorption range and facilitate charge carrier dynamics. Nano Energy, 2015, 18: 222–231
22. Shi W, Zhang X, Brillet J, Huang D, Li M, Wang M, Shen Y. Significant enhancement of the photoelectrochemical activity of WO_3 nanoflakes by carbon quantum dots decoration. Carbon, 2016, 105: 387–393
23. Kim T W, Choi K S. Nanoporous $BiVO_4$ photoanodes with dual-layer oxygen evolution catalysts for solar water splitting. Science, 2014, 343(6174): 990–994
24. Wang J C, Yao H C, Fan Z Y, Zhang L, Wang J S, Zang S Q, Li Z J. Indirect Z-scheme BiOI/g-C_3N_4 photocatalysts with enhanced photoreduction CO_2 activity under visible light irradiation. ACS Applied Materials & Interfaces, 2016, 8(6): 3765–3775
25. Li W, Da P, Zhang Y, Wang Y, Lin X, Gong X, Zheng G. WO_3 nanoflakes for enhanced photoelectrochemical conversion. ACS Nano, 2014, 8(11): 11770–11777
26. Nonaka K, Takase A, Miyakawa K. Raman spectra of sol-gel-derived tungsten oxides. Journal of Materials Science Letters, 1993, 12(5): 274–277
27. Cui X, Zhang H, Dong X, Chen H, Zhang L, Guo L, Shi J. Electrochemical catalytic activity for the hydrogen oxidation of mesoporous WO_3 and WO_3/C composites. Journal of Materials Chemistry, 2008, 18(30): 3575–3580
28. Sun Y, Murphy C J, Reyes-Gil K R, Reyes-Garcia E A, Thornton J M, Morris N A, Raftery D. Photoelectrochemical and structural characterization of carbon-doped WO_3 films prepared via spray pyrolysis. International Journal of Hydrogen Energy, 2009, 34(20): 8476–8484
29. Chang C, Zhu L, Wang S, Chu X, Yue L. Novel mesoporous graphite carbon nitride/BiOI heterojunction for enhancing photocatalytic performance under visible-light irradiation. ACS Applied Materials & Interfaces, 2014, 6(7): 5083–5093
30. Zhang Y, Pei Q, Liang J, Feng T, Zhou X, Mao H, Zhang W, Hisaeda Y, Song X M. Mesoporous TiO_2-based photoanode sensitized by BiOI and investigation of its photovoltaic behavior. Langmuir, 2015, 31(37): 10279–10284
31. Feng Y, Liu C, Che H, Chen J, Huang K, Huang C, Shi W. The highly improved visible light photocatalytic activity of BiOI through fabricating a novel p–n heterojunction BiOI/WO_3 nanocomposite. CrystEngComm, 2016, 18(10): 1790–1799
32. Hou Y, Zuo F, Dagg A P, Liu J, Feng P. Branched WO_3 nanosheet array with layered C_3N_4 heterojunctions and CoO_x nanoparticles as a flexible photoanode for efficient photoelectrochemical water oxidation. Advanced Materials, 2014, 26(29): 5043–5049

Weina Shi received her B.S. and M.S. degrees in Chemistry from Zhengzhou University in 2010 and 2013, respectively, and her Ph.D. degree in the Wuhan National Laboratory for Optoelectronics in 2016 from Huazhong University of Science and Technology. In 2017, she works at Xinxiang University. Her research interests include photocatalysis and photoelectrocatalysis.

Xiaowei Lv is currently pursuing his Ph.D. degree under the supervision of Prof. Yan Shen in the Wuhan National Laboratory for Optoelectronics, Huazhong University of Science and Technology, China. His research interests focus on the design and development of high performance semconductor materials and their potential applications in (photo)electrocatalytic water splitting.

Yan Shen received her Ph.D. degree from the Changchun Institute of Applied Chemistry, Chinese Academy of Sciences in 2003. From 2004 to 2006, she was an Alexander von Humboldt Fellow and Hanse-Wissenschaftskolleg (HWK) fellow successively in the group of Prof. Gunther Wittstock at the University of Oldenburg. She became a professor at Harbin Institute of Technology in 2009. Currently, she works as a professor at Wuhan National Laboratory for Optoelectronics. Her research interests include electrochemistry related to energy conversion and storage, photoelectrochemical water splitting, and investigation of local reactions at solid-liquid interfaces.